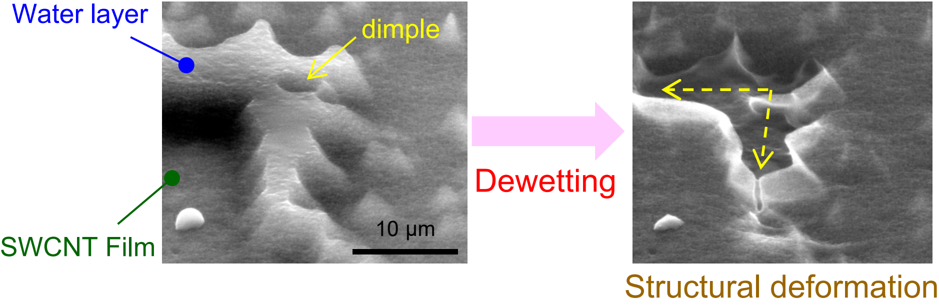
Water layer
dimple
SWCNT Film
10 μm
Dewetting
Structural deformation

In situ observation of dewetting-induced deformation of vertically aligned single-walled carbon nanotubes

Yuta Yoshimoto[a], Koichi Isomura[a], Sou Sugiyama[a], Hua An[a], Takuma Hori[b], Taiki Inoue[a], Shohei Chiashi[a], Shu Takagi[a], Shigeo Maruyama[a, c, *], Ikuya Kinefuchi[a, *]

[a] *Department of Mechanical Engineering, The University of Tokyo, 7-3-1 Hongo, Bunkyo-ku, Tokyo 113-8656, Japan*

[b] *Department of Mechanical Engineering, Tokyo University of Science, 2641 Yamazaki, Noda, Chiba 278-8510, Japan*

[c] *Energy NanoEngineering Laboratory, National Institute of Advanced Industrial Science and Technology (AIST), 1-2-1 Namiki, Tsukuba 305-8564, Japan*

[*] Corresponding authors.
E-mail addresses: maruyama@photon.t.u-tokyo.ac.jp (S. Maruyama), kine@fel.t.u-tokyo.ac.jp (I. Kinefuchi).

ABSTRACT

We investigated dynamical processes of capillary-mediated deformation of vertically aligned single-walled carbon nanotubes (VA-SWCNTs) via *in situ* observation of their wetting and dewetting behaviors using an environmental scanning electron microscope (ESEM). Three types of wetting behaviors on a VA-SWCNT sample were confirmed, including conical shaped water aggregates, spherical droplets on tips of conical shaped water aggregates, and extensively distributed water layers. While the former two types both resulted in dimples on the VA-SWCNT surface and failed to induce large-scale deformation of VA-SWCNTs, the latter caused the formation of wall-like structures and crack propagation in the VA-SWCNT film during the dewetting process due to directional retraction of vapor-liquid interfaces. This dewetting-induced large-scale deformation that was confirmed by the *in situ* ESEM observation for the first time represented initial stages of capillary processes, leading to the self-organization of VA-SWCNTs reported in recent literatures. Compared to the previous studies based on *ex situ* observations of dried samples, our *in situ* observation successfully captured temporal evolution of the dewetting-induced deformation, facilitating the more precise construction of predictive models of final morphologies of VA-SWCNT films after capillary-mediated densification.

Keywords: Single-walled carbon nanotubes; Dewetting; *In situ* observation; Environmental scanning electron microscope

1. Introduction

Carbon nanotubes (CNTs) [1,2] possess excellent electrical [3], optical [4], mechanical [5], and thermal properties [6]. CNTs, thus, have been widely studied for various applications. In addition to nanostructures of an individual CNT, there is a need to control macroscale morphologies of CNT ensembles, which depends on intended applications. For instance, horizontally aligned CNTs [7] are suitable for field-effect transistors [8], while vertically aligned (VA-) CNTs [9,10] are efficiently used for thermal interface materials [11]. The morphology of VA-CNTs can be further adjusted via post-growth processing. Capillary-mediated self-organization of VA-CNTs [12,13] is one of the attractive approaches in terms of its scalability and low-cost. Such a simple liquid-induced process has realized various CNT morphologies by tuning original VA-CNTs and treatment methods, such as honeycomb-like networks [12,13], tepee structures [14], densified arrays [15], and more complex architectures [15,16]. These shape-engineered CNTs have demonstrated their superior performance as cell seeding scaffolds [17], field-emitters [18], super-capacitors [15], sliding electrical contacts [19], and CNT-Si heterojunction solar cells [20].

In general, when nanopillars such as VA-CNTs are immersed in water and pierce the vapor-liquid interface, capillary force causes nanopillars to bend and buckle [21–26], resulting in their collapse or clustering [27]. Some studies have proposed predictive models for the final morphology of VA-CNTs after capillary-mediated densification [27,28]. However, most studies to date have been based on *ex situ* observations of the dried structures [12,16,19,29], paying much less attention to dynamical processes of VA-CNT deformation during wetting and dewetting. The elucidation of these dynamical processes can contribute to constructing more precise models that enable the prediction of the final morphology according to experimental conditions; therefore, allowing the opportunity to tailor morphologies for certain purpose. However, it is still a challenge to observe microscale dynamical processes of the VA-CNT deformation using an optical microscope via conventional direct immersion of VA-CNTs in water [12,30] or exposure of VA-CNTs to vapor [16,19,29]. Therefore, the present study aims to capture the dynamical processes of the capillary-mediated deformation of vertically aligned single-walled carbon nanotubes (VA-SWCNTs) by *in situ* observation of their wetting and dewetting behaviors using an environmental scanning electron microscope (ESEM). The formation of wall-like structures and crack propagation in a VA-SWCNT film during the dewetting process of water were confirmed, which supports the initial stage of capillary-mediated modifications of VA-SWCNT morphologies.

2. Materials and methods

2.1. Vertically aligned single-walled carbon nanotubes (VA-SWCNTs)

VA-SWCNTs were synthesized on a Co/Mo dip-coated Si/SiO_2 substrate using the alcohol catalytic chemical vapor deposition process [10,31], as shown in Fig. 1. The high *G*/*D* ratio obtained by the Raman spectroscopy (see Supplementary material S1) ensured the high quality of the VA-SWCNTs. The average diameter of the VA-SWCNTs and the film thickness were about 2 nm and 5 μm, respectively. The number density of the VA-SWCNTs was ~ 10^{12} cm^{-2}, leading to the porosity of ~ 97% [32]. The VA-SWCNT film had a disordered and dense crust layer on the top region [33].

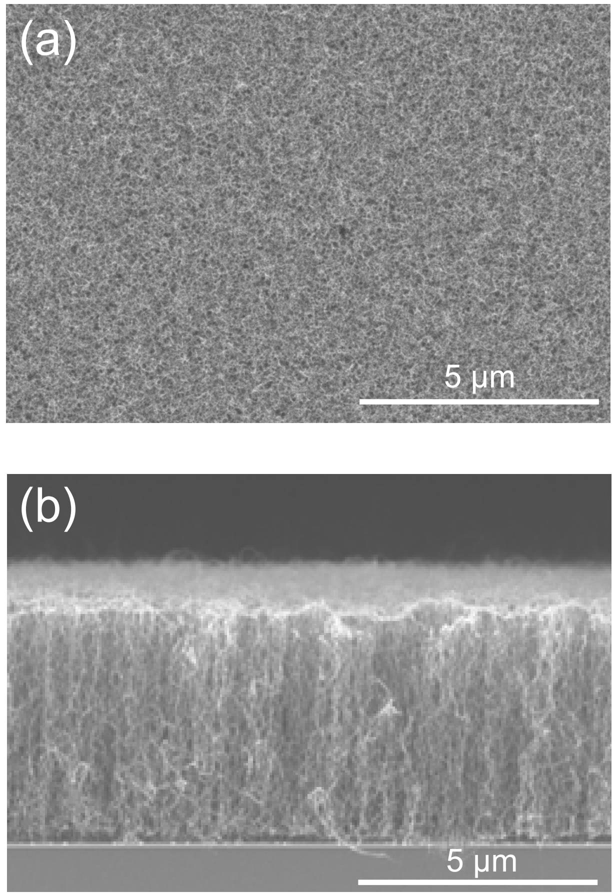

Fig. 1. Scanning electron microscope (SEM) images of the VA-SWCNT film from a top view (a) and a side view (b).

2.2. Experimental identification of water-induced deformation of VA-SWCNTs

It was reported that the exposure of VA-CNTs to vapor results in self-assembled microhoneycomb networks [20], although its microscale dynamical processes are yet to be understood (see Supplementary material S2). In the present study, we employed an environmental scanning electron microscope (ESEM, FEI Quanta 250) for the *in situ* observation of water-induced deformation of VA-SWCNTs, as illustrated in Fig. 2. The sample was mounted on a copper holder in contact with a Peltier cooling stage at 1.0 °C. The sample was tilted by 65° with respect to the horizontal direction to observe the water distribution and shapes of water aggregates on the sample. The ambient temperature inside the vacuum chamber, except in the vicinity of the sample, was about 23 °C (i.e., room temperature). The working distance was 3 mm. The acceleration voltage and the probe current were 20 kV and 0.28 nA, respectively. The pressure of water vapor was initially kept at $P \approx 680$ Pa and elevated to $P \approx 760$ Pa to initiate the vapor condensation. Subsequently, the vapor pressure was reduced to $P \approx 680$ Pa to induce the water evaporation. This pressure range roughly originated from the saturation vapor pressure (657 Pa) at 1 °C [34], although a larger pressure was actually required to trigger vapor condensation on the VA-SWCNT film because the film temperature was higher than that of the Peltier cooling stage.

Note that before measurements, almost all gases in the chamber were purged by water vapor through purge-flood cycles, ensuring that the fraction of non-condensable gases was lower than 1%. Then, the water vapor pressure inside the chamber was controlled via the microscope's feedback control system.

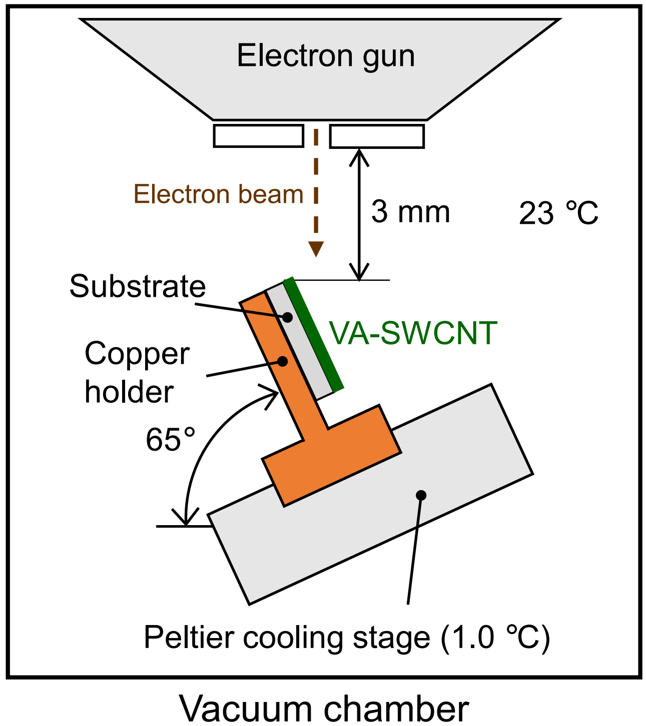

Fig. 2. A schematic presentation of the ESEM measurement system. The sample was mounted on a copper holder in contact with a cooling stage at 1.0 °C via a Peltier cooling system. The sample was tilted by 65° with respect to the horizontal direction. The ambient temperature inside the chamber was about 23 °C. Dimensions are not to scale.

After the *in situ* observation of the VA-SWCNT deformation induced by water vapor condensation and evaporation, a scanning electron microscope (SEM) (Hitachi High-Tech, S-4800) was also employed to complement the observation.

3. Results and discussion

Figure 3 shows water aggregates condensing on the sample at the vapor pressure of $P \approx 760$ Pa in the ESEM chamber. Water aggregates under the crust layer were visible because the VA-SWCNT film was transparent, owing to its high porosity (~ 97%) which allowed the electron beam (secondary electrons) to enter inside (escape from) the film. The bottom left region bounded by the green dashed-dotted line was initially exposed to electron beams for observation, followed by the change of view. Clearly, there was negligible condensed water in the initial observation area due to electron beam heating effects [35,36]. Meanwhile, an evident amount of water aggregates were found at the boundary of the initial observation area swept by the electron beam. In addition, a number of small water aggregates were observed out of the initial observation area. Three types of wetting behaviors on the VA-SWCNT sample were confirmed, including (I) conical shaped water aggregates, (II) spherical droplets on the tips of conical shaped water aggregates, and (III) extensively distributed water layers. While the water aggregates of types (I) and (II) were mainly observed out of the initial observation area, the water layers were only observed along the edge of that area. We infer that this intriguing phenomenon originates from the balance between suppression and enhancement effects of vapor condensation by electron beams. While heating effects due to electron beams [35,36] suppressed vapor condensation, positively charged water molecules (H_2O^+) in the ESEM chamber interacted with negatively charged surfaces [37] and became H_2O, enhancing the nucleation of liquid water. Specifically, the boundary of the initial observation area was exposed to more electron beams because of the turnarounds of the electron beam sweep. Vapor condensation, thus, was enhanced and overwhelmed the evaporation due to heating effects. This allowed for the formation of extensively distributed water layers (III) in the ESEM environment. For the water aggregates of type (I), the nucleation was considered to occur at the interface between the substrate and VA-SWCNTs (Fig. 2), where the temperature was lower than that at the tips of VA-SWCNTs. The condensation growth subsequently proceeded upwards until the crust region was reached, which suppressed further growth in the height direction. The type (II) may originate from type (I), i.e., water aggregates of type (I) turned to be type (II) after penetrating through the crust region. As we discuss below, the extensively distributed water layers (III) mainly contributed to the formation of wall-like structures and crack propagation.

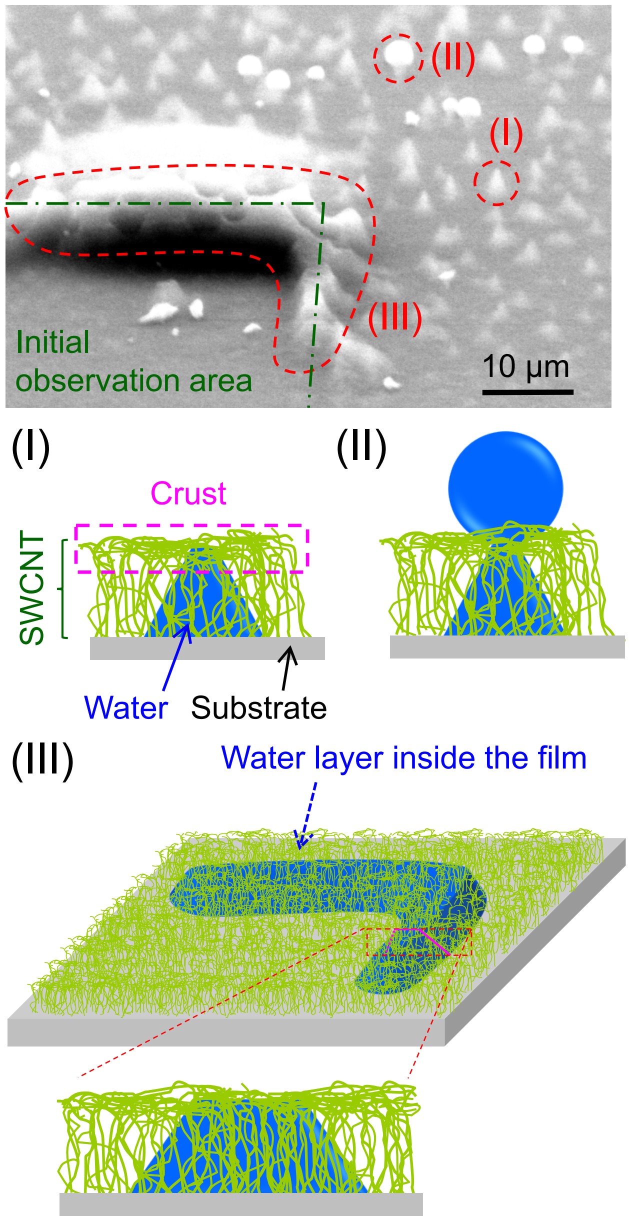

Fig. 3. Wetting behaviors of VA-SWCNTs observed in the ESEM chamber having the vapor pressure of $P \approx 760$ Pa. Water aggregates under the crust layer were visible because of high porosity of the VA-SWCNT film. Three types of wetting behaviors were exhibited, i.e., (I)

conical shaped water aggregates, (II) spherical droplets on the tips of conical shaped water aggregates, and (III) extensively distributed water layers inside the VA-SWCNT forest. The bottom left area bounded by the green dashed-dotted line was initially exposed to electron beams for observation.

Figure 4 shows the type (III) wetting behavior of VA-SWCNTs during vapor condensation observed in the ESEM chamber. VA-SWCNTs became evidently wet for the pressure of $P \approx 760$ Pa, exhibiting extensively distributed water layers as discussed above. We note that there was no evident structural deformation of the VA-SWCNTs during the wetting process for more than 5 min. In contrast, structural deformation of the VA-SWCNTs was clearly confirmed during the dewetting process, as shown in Fig. 5. By decreasing the pressure to $P \approx 680$ Pa, a dimple appeared in wet SWCNTs as shown in Fig. 5(a). Subsequently, vapor-liquid interfaces retracted from the dimple along the edges of the initial observation area (Fig. 3) as indicated by the dashed arrows in Figs. 5(b)–(f), generating structural deformations of SWCNTs along these directions. This directional retraction of the vapor-liquid interfaces played a key role in the large-scale structural deformation of VA-SWCNTs.

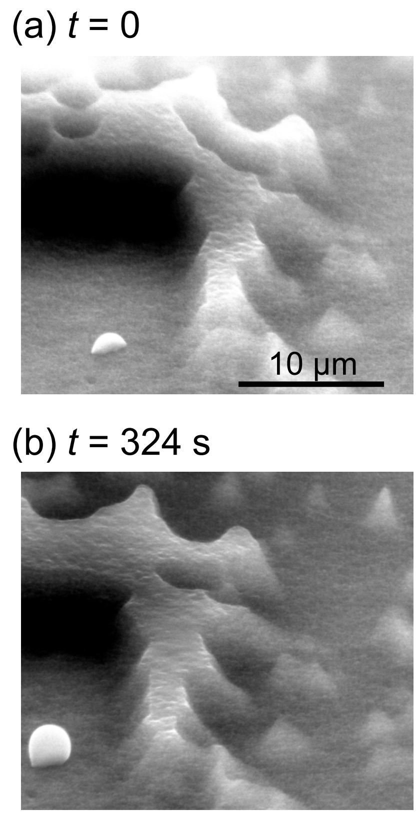

Fig. 4. The type (III) wetting behavior of the VA-SWCNTs during vapor condensation observed in the ESEM chamber having the vapor pressure of $P \approx 760$ Pa; (a) $t = 0$ s, (b) $t = 324$ s.

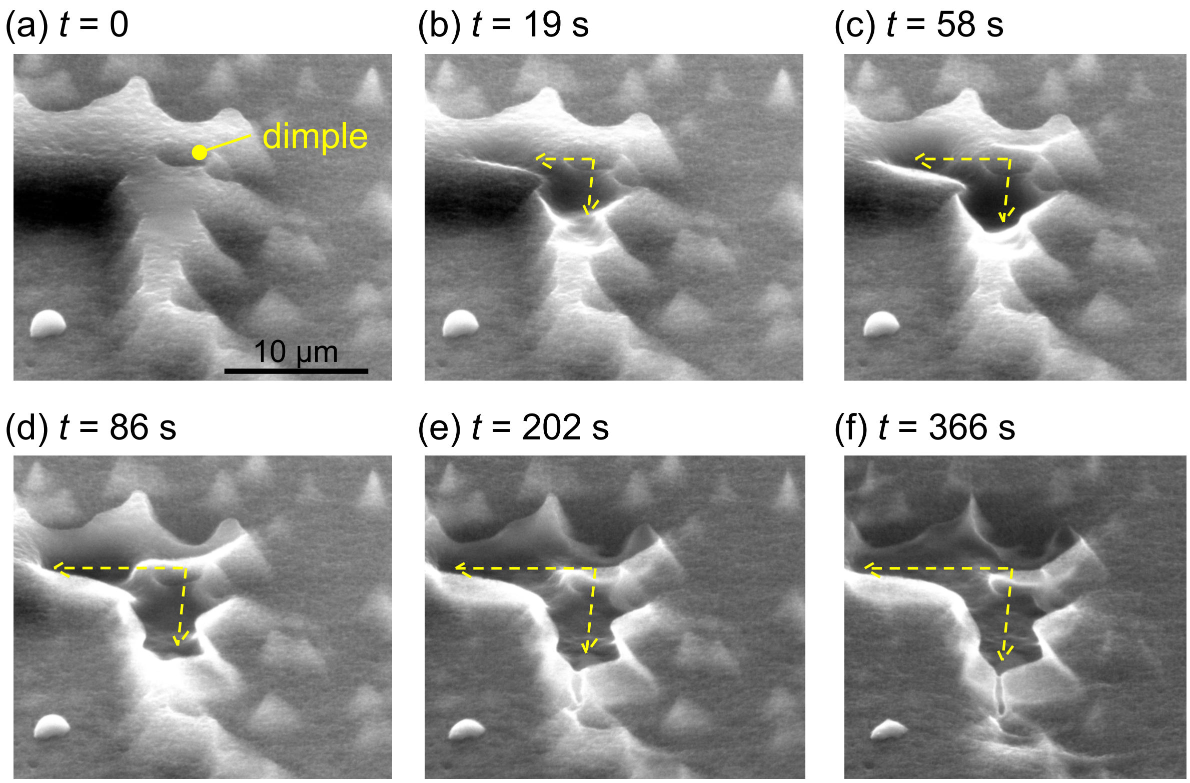

Fig. 5. Time evolution of dewetting-induced deformation of the VA-SWCNTs during evaporation of an extensively distributed water layer (the type (III) in Fig. 3) observed in the ESEM chamber having the vapor pressure of $P \approx 680$ Pa; (a) $t = 0$ s, (b) $t = 19$ s, (c) $t = 58$ s, (d) $t = 86$ s, (e) $t = 202$ s, (f) $t = 366$ s. The dashed arrows in (b)–(f) represent the directions of structural deformations.

To investigate the dewetting-induced deformation of the VA-SWCNTs in detail, Fig. 6 compares the *in situ* ESEM image with the subsequent SEM images after the exposure to vapor. As shown in Fig. 6(b), collapsed SWCNTs were clearly observed. In addition, crack and wall-like structures were also confirmed in Figs. 6(c) and (d). Again, extensively distributed water layers (III) played an important role to induce large-scale deformation of the SWCNTs, resulting in the collapse, crack propagation, and formation of wall-like structures.

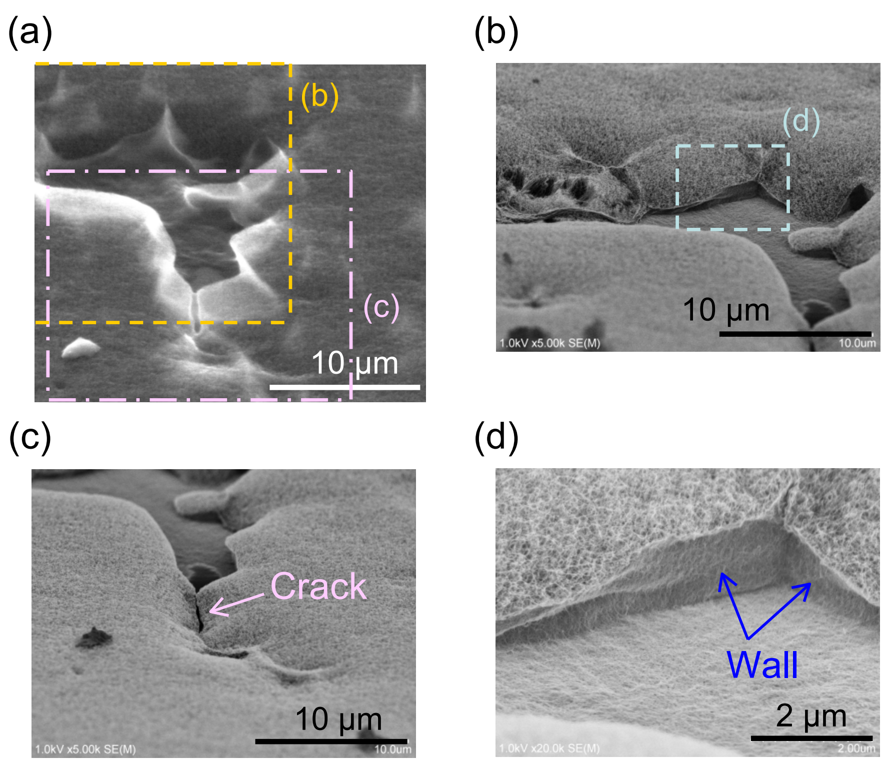

Fig. 6. Specification of dewetting-induced deformation of SWCNTs by comparing the *in situ*

ESEM image (a) with the subsequent SEM images after the exposure to vapor (b–d). The SEM observation angle was 65° in accordance with the ESEM observation. (a) ESEM image identical to Fig. 5(f). (b) SEM image corresponding to the region denoted by the dashed line in (a); (c) SEM image of the crack corresponding to the region denoted by the dashed-dotted line in (a); (d) SEM image of the wall-like structure corresponding to the region denoted by the dashed line in (b).

Figure 7 shows the SEM images of the SWCNTs where the water aggregates of types (I) and (II) were present. While a number of dimples were present on the SWCNT surface, large-scale structural deformation of the SWCNTs was not confirmed, which is different from the area where the water layers (III) were extensively distributed. Basically, VA-SWCNTs that pierce a vapor-liquid interface are subject to a compressive force along the thickness and hence likely to buckle [27,38]. More specifically, for a circular rod clamped on a substrate, the critical buckling length is given by

$$L_\mathrm{c} = \frac{\pi}{2}\sqrt{\frac{EI}{F_\mathrm{cap}}} \tag{1}$$

where $E \sim 1$ TPa is Young's modulus of a single SWCNT [39], $I = \pi r^4/4$ is inertia moment with SWCNT radius of $r \sim 2$ nm, $F_\mathrm{cap} = 2\pi r\cos\theta$ is capillary force with surface tension of $\gamma \approx 72$

mN/m and contact angle of $\theta \approx 86^{\circ}$ corresponding to a water droplet on a graphite surface [40]. Equation 1 yielded $L_c \approx 0.7$ μm < $H \approx 5$ μm with H being the SWCNT length. The possibility of the SWCNT buckling, thus, was indicated. However, entanglements and crust regions together with the small amount of water prevented complete collapse of SWCNTs in the present conditions. In addition, no clear difference in the deformed structures was observed between the spots where the water aggregates of types (I) and (II) were present. Namely, both of type (I) and (II) water aggregates just yielded dimples and failed to induce large-scale deformation of the VA-SWCNTs in contrast to type (III). Directional retraction of vapor-liquid interfaces of spatially distributed water layers (Fig. 5) played a crucial role for the large-scale deformation of VA-SWCNTs, leading to crack propagation and formation of wall-like structures. Although the extensively distributed water layers observed in the present study stemmed from the vapor condensation enhancement due to electron beams, we expect that the directional retraction of their vapor-liquid interfaces could be a main factor of spatially distributed deformation of VA-SWCNTs in actual capillary process.

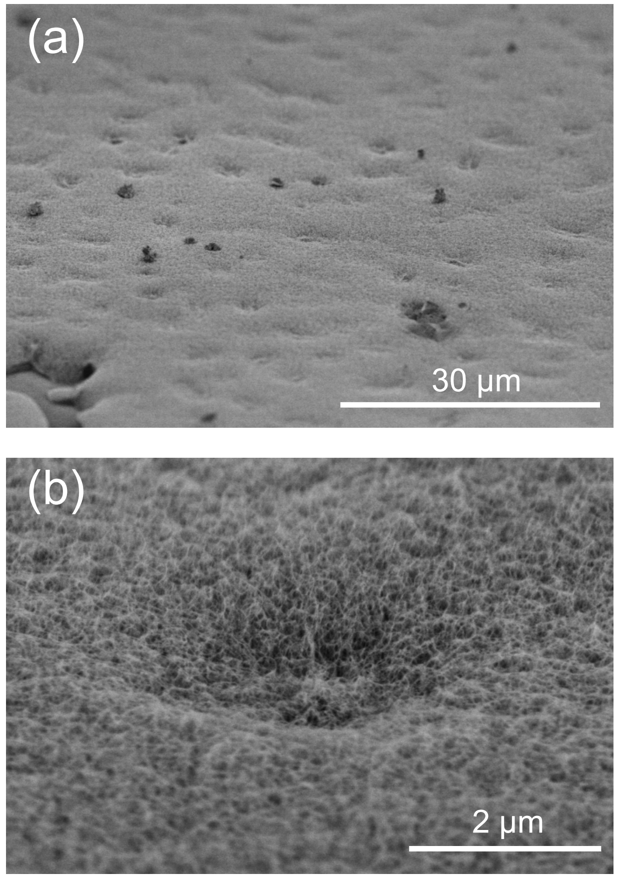

Fig. 7. SEM images of the SWCNTs where the water aggregates of types (I) and (II) were present in Fig. 3. The SEM observation angle was 65° in accordance with the ESEM observation (Fig. 2). (a) Dimples distributed on the SWCNT surface. (b) Enlarged view of a representative dimple.

Finally, self-assembled microhoneycomb networks reported by Cui et al. [20] were not observed in the present study. We note that the water vapor treatment [20] consisted of repetitive two steps, i.e., (1) exposing a VA-SWCNT array to vapor from a hot water reservoir and (2) turning the sample over and drying the array in an ambient environment (see Supplementary material S2), which is considerably different from our experimental condition.

4. Conclusions

We investigated dynamical processes of capillary-mediated deformation of vertically aligned single-walled carbon nanotubes (VA-SWCNTs) by *in situ* observation of their wetting and dewetting behaviors using an environmental scanning electron microscope (ESEM). We confirmed the formation of wall-like structures and crack propagation in the VA-SWCNT film during the dewetting process of water, which were caused by extensively distributed water layers that resulted in directional retraction of vapor-liquid interfaces. Such dewetting-induced large-scale deformation that was for the first time captured by the *in situ* ESEM observation represented initial stages of capillary processes, leading to capillary-mediated self-organization of VA-SWCNTs. Our findings can help to more precisely construct the predictive models of final morphologies of VA-SWCNT films after capillary-mediated densification. Finally, it will be interesting to use SWCNT films with microscale patterns fabricated via a lithography process [38]. The pre-patterned surfaces would allow us to control the directions of SWCNT deformation, enabling more systematic *in situ* observation of the dewetting-induced deformation using an ESEM.

Acknowledgments

This work was partly supported by JSPS KAKENHI Grant Numbers JP15H05760 and JP18H05329.

Appendix A. Supplementary data

Supplementary data to this article can be found online at ***.

References

[1] S. Iijima, Helical microtubules of graphitic carbon, Nature. 354 (1991) 56–58. doi:10.1038/354056a0.

[2] S. Iijima, T. Ichihashi, Single-shell carbon nanotubes of 1-nm diameter, Nature. 363 (1993) 603–605. doi:10.1038/363603a0.

[3] Z. Yao, C.L. Kane, C. Dekker, High-Field Electrical Transport in Single-Wall Carbon Nanotubes, Phys. Rev. Lett. 84 (2000) 2941–2944. doi:10.1103/PhysRevLett.84.2941.

[4] M.J. O'Connell, S.M. Bachilo, C.B. Huffman, V.C. Moore, M.S. Strano, E.H. Haroz, K.L. Rialon, P.J. Boul, W.H. Noon, C. Kittrell, J. Ma, R.H. Hauge, R.B. Weisman, R.E. Smalley, Band gap fluorescence from individual single-walled carbon nanotubes, Science. 297 (2002) 593–596. doi:10.1126/science.1072631.

[5] M.-F. Yu, O. Lourie, M.J. Dyer, K. Moloni, T.F. Kelly, R.S. Ruoff, Strength and breaking mechanism of multiwalled carbon nanotubes under tensile load, Science. 287 (2000) 637–640. doi:10.1126/SCIENCE.287.5453.637.

[6] P. Kim, L. Shi, A. Majumdar, P.L. McEuen, Thermal Transport Measurements of Individual Multiwalled Nanotubes, Phys. Rev. Lett. 87 (2001) 215502. doi:10.1103/PhysRevLett.87.215502.

[7] C. Kocabas, S.-H. Hur, A. Gaur, M.A. Meitl, M. Shim, J.A. Rogers, Guided Growth of Large-Scale, Horizontally Aligned Arrays of Single-Walled Carbon Nanotubes and Their Use in Thin-Film Transistors, Small. 1 (2005) 1110–1116. doi:10.1002/smll.200500120.

[8] S.J. Kang, C. Kocabas, T. Ozel, M. Shim, N. Pimparkar, M.A. Alam, S. V. Rotkin, J.A. Rogers, High-performance electronics using dense, perfectly aligned arrays of single-walled carbon nanotubes, Nat. Nanotechnol. 2 (2007) 230–236. doi:10.1038/nnano.2007.77.

[9] W.Z. Li, S.S. Xie, L.X. Qian, B.H. Chang, B.S. Zou, W.Y. Zhou, R.A. Zhao, G. Wang, Large-Scale Synthesis of Aligned Carbon Nanotubes, Science. 274 (1996) 1701–1703. doi:10.1126/SCIENCE.274.5293.1701.

[10] Y. Murakami, S. Chiashi, Y. Miyauchi, M. Hu, M. Ogura, T. Okubo, S. Maruyama, Growth of vertically aligned single-walled carbon nanotube films on quartz substrates and their optical anisotropy, Chem. Phys. Lett. 385 (2004) 298–303. doi:10.1016/J.CPLETT.2003.12.095.

[11] J. Xu, T.S. Fisher, Enhanced thermal contact conductance using carbon nanotube array interfaces, IEEE Trans. Components Packag. Technol. 29 (2006) 261–267. doi:10.1109/TCAPT.2006.875876.

[12] H. Liu, S. Li, J. Zhai, H. Li, Q. Zheng, L. Jiang, D. Zhu, Self-Assembly of Large-Scale Micropatterns on Aligned Carbon Nanotube Films, Angew. Chemie Int. Ed. 43 (2004) 1146–1149. doi:10.1002/anie.200351988.

[13] N. Chakrapani, B. Wei, A. Carrillo, P.M. Ajayan, R.S. Kane, Capillarity-driven assembly of two-dimensional cellular carbon nanotube foams, Proc. Natl. Acad. Sci. U. S. A. 101 (2004) 4009–4012. doi:10.1073/pnas.0400734101.

[14] K.K.S. Lau, J. Bico, K.B.K. Teo, M. Chhowalla, G.A.J. Amaratunga, W.I. Milne, G.H.

McKinley, K.K. Gleason, Superhydrophobic Carbon Nanotube Forests, Nano Lett. 3 (2003) 1701–1705. doi:10.1021/NL034704T.

[15] D.N. Futaba, K. Hata, T. Yamada, T. Hiraoka, Y. Hayamizu, Y. Kakudate, O. Tanaike, H. Hatori, M. Yumura, S. Iijima, Shape-engineerable and highly densely packed single-walled carbon nanotubes and their application as super-capacitor electrodes, Nat. Mater. 5 (2006) 987–994. doi:10.1038/nmat1782.

[16] M. De Volder, S.H. Tawfick, S.J. Park, D. Copic, Z. Zhao, W. Lu, A.J. Hart, Diverse 3D Microarchitectures Made by Capillary Forming of Carbon Nanotubes, Adv. Mater. 22 (2010) 4384–4389. doi:10.1002/adma.201001893.

[17] M.A. Correa-Duarte, N. Wagner, J. Rojas-Chapana, C. Morsczeck, M. Thie, M. Giersig, Fabrication and Biocompatibility of Carbon Nanotube-Based 3D Networks as Scaffolds for Cell Seeding and Growth, Nano Lett. 4 (2004) 2233–2236. doi:10.1021/NL048574F.

[18] L.M. Sheng, M. Liu, P. Liu, Y. Wei, L. Liu, S.S. Fan, Field emission from self-assembly structure of carbon-nanotube films, Appl. Surf. Sci. 250 (2005) 9–13. doi:10.1016/J.APSUSC.2004.12.036.

[19] D.N. Futaba, K. Miyake, K. Murata, Y. Hayamizu, T. Yamada, S. Sasaki, M. Yumura, K. Hata, Dual Porosity Single-Walled Carbon Nanotube Material, Nano Lett. 9 (2009) 3302–

3307. doi:10.1021/nl901581t.

[20] K. Cui, T. Chiba, S. Omiya, T. Thurakitseree, P. Zhao, S. Fujii, H. Kataura, E. Einarsson, S. Chiashi, S. Maruyama, Self-Assembled Microhoneycomb Network of Single-Walled Carbon Nanotubes for Solar Cells, J. Phys. Chem. Lett. 4 (2013) 2571–2576. doi:10.1021/jz401242a.

[21] D. Chandra, S. Yang, Capillary-Force-Induced Clustering of Micropillar Arrays: Is It Caused by Isolated Capillary Bridges or by the Lateral Capillary Meniscus Interaction Force?, Langmuir. 25 (2009) 10430–10434. doi:10.1021/la901722g.

[22] C.-C. Chang, Z. Wang, Y.-J. Sheng, H.-K. Tsao, Nanostructure collapse by elasto-capillary instability, Soft Matter. 10 (2014) 8542–8547. doi:10.1039/C4SM01520G.

[23] P.A. Kralchevsky, V.N. Paunov, I.B. Ivanov, K. Nagayama, Capillary meniscus interaction between colloidal particles attached to a liquid–fluid interface, J. Colloid Interface Sci. 151 (1992) 79–94. doi:10.1016/0021-9797(92)90239-I.

[24] C. Py, R. Bastien, J. Bico, B. Roman, A. Boudaoud, 3D aggregation of wet fibers, Europhys. Lett. 77 (2007) 44005. doi:10.1209/0295-5075/77/44005.

[25] D. Chandra, S. Yang, Stability of High-Aspect-Ratio Micropillar Arrays against Adhesive and Capillary Forces, Acc. Chem. Res. 43 (2010) 1080–1091. doi:10.1021/ar100001a.

[26] B. Roman, J. Bico, Elasto-capillarity: deforming an elastic structure with a liquid droplet, J. Phys. Condens. Matter. 22 (2010) 493101. doi:10.1088/0953-8984/22/49/493101.

[27] F. Chiodi, B. Roman, J. Bico, Piercing an interface with a brush: Collaborative stiffening, EPL. 90 (2010) 44006. doi:10.1209/0295-5075/90/44006.

[28] A.L. Kaiser, I.Y. Stein, K. Cui, B.L. Wardle, Process-morphology scaling relations quantify self-organization in capillary densified nanofiber arrays, Phys. Chem. Chem. Phys. 20 (2018) 3876–3881. doi:10.1039/C7CP06869G.

[29] M.F.L. De Volder, S.J. Park, S.H. Tawfick, D.O. Vidaud, A.J. Hart, Fabrication and electrical integration of robust carbon nanotube micropillars by self-directed elastocapillary densification, J. Micromechanics Microengineering. 21 (2011) 045033. doi:10.1088/0960-1317/21/4/045033.

[30] C.T. Wirth, S. Hofmann, J. Robertson, Surface properties of vertically aligned carbon nanotube arrays, Diam. Relat. Mater. 17 (2008) 1518–1524. doi:10.1016/j.diamond.2007.11.019.

[31] S. Maruyama, R. Kojima, Y. Miyauchi, S. Chiashi, M. Kohno, Low-temperature synthesis of high-purity single-walled carbon nanotubes from alcohol, Chem. Phys. Lett. 360 (2002) 229–234. doi:10.1016/S0009-2614(02)00838-2.

[32] R. Xiang, Z. Yang, Q. Zhang, G. Luo, W. Qian, F. Wei, M. Kadowaki, E. Einarsson, S. Maruyama, Growth Deceleration of Vertically Aligned Carbon Nanotube Arrays: Catalyst Deactivation or Feedstock Diffusion Controlled?, J. Phys. Chem. C. 112 (2008) 4892–4896. doi:10.1021/JP710730X.

[33] Y. Won, Y. Gao, M.A. Panzer, R. Xiang, S. Maruyama, T.W. Kenny, W. Cai, K.E. Goodson, Zipping, entanglement, and the elastic modulus of aligned single-walled carbon nanotube films, Proc. Natl. Acad. Sci. U. S. A. 110 (2013) 20426–20430. doi:10.1073/pnas.1312253110.

[34] D.R. Lide, CRC Handbook of Chemistry and Physics, 85th ed., CRC Press, Boca Raton, Florida, 2004.

[35] R.E. Cameron, A.M. Donald, Minimizing sample evaporation in the environmental scanning electron microscope, J. Microsc. 173 (1994) 227–237. doi:10.1111/j.1365-2818.1994.tb03445.x.

[36] K. Rykaczewski, J.H.J. Scott, A.G. Fedorov, Electron beam heating effects during environmental scanning electron microscopy imaging of water condensation on superhydrophobic surfaces, Appl. Phys. Lett. 98 (2011) 093106. doi:10.1063/1.3560443.

[37] G.D. Danilatos, Foundations of Environmental Scanning Electron Microscopy, Adv.

Electron. Electron Phys. 71 (1988) 109–250. doi:10.1016/S0065-2539(08)60902-6.

[38] S.H. Tawfick, J. Bico, S. Barcelo, Three-dimensional lithography by elasto-capillary engineering of filamentary materials, MRS Bull. 41 (2016) 108–114. doi:10.1557/mrs.2016.4.

[39] A. Sears, R.C. Batra, Macroscopic properties of carbon nanotubes from molecular-mechanics simulations, Phys. Rev. B. 69 (2004) 235406. doi:10.1103/PhysRevB.69.235406.

[40] A.W. Adamson, A.P. Gast, Physical Chemistry of Surfaces, 6th ed., Wiley, New York, 1997.